

**Tuning electronic structure of MOF-based solid-state electrolytes to activate dormant lithium and facilitate ion transport kinetics towards lithium metal batteries**

Qing Liu,<sup>a</sup> Qi An,<sup>a</sup> Kun Zeng,<sup>a</sup> Mou Yang,<sup>a</sup> Haiye Zhu,<sup>a</sup> Xilin Liang,<sup>a</sup> Guiquan Zhao,<sup>a</sup>

Mengjiao Sun,<sup>a</sup> Yunchun Zha,<sup>a</sup> Li Yang,<sup>a</sup> Lingyan Duan,<sup>a</sup> Genfu Zhao,<sup>a</sup> Yongjiang Sun,<sup>a</sup>

Hong Guo,<sup>a, b, \*</sup>

<sup>a</sup> School of Materials and Energy, Yunnan University, Kunming 650091, China

<sup>b</sup> Southwest United Graduate School, Kunming 650091, China

\*Corresponding author:

guohong@ynu.edu.cn (Hong Guo)

## **Experimental Section**

### **Synthesis of MIL-125(Ti)**

MIL-125 was synthesized using a straightforward hydrothermal method. Initially, 1.12 g of 2-amino-terephthalic acid was dissolved in a mixture of 72 mL dimethylformamide (DMF) and 8 mL methanol, followed by stirring for 30 minutes to ensure complete dissolution. Subsequently, 1.38 mL of tetrabutyl titanate was added to the homogeneous solution and stirred for an additional hour. The well-mixed solution was then transferred to a 150 mL autoclave and subjected to hydrothermal treatment at 150 ° C for 24 hours. Upon completion, the sample was thoroughly washed with DMF and methanol to remove impurities and dried at 60 ° C to eliminate residual solvents, yielding pure white MIL-125 powder.

### **Synthesis of gel electrolyte precursor**

215.30 mg of LiTFSI, 35.15 mg of LiBF<sub>4</sub>, and 1.5 mg of MOF were initially dissolved in 1 mL of DOL (analytical reagent grade), followed by stirring for 1 hour to ensure homogeneity. Subsequently, 0.5 mL of a polymerization initiator solution containing 1 M LiPF<sub>6</sub> in a 1:1 ethylene carbonate (EC) and dimethyl ether (DME) mixture was added, and the combined solution was stirred at 25 °C for an additional 30 minutes. This resulting solution served as the gel electrolyte precursor for battery assembly.

### **Synthesis of the electrodes**

The cathode employed commercial LiCoO<sub>2</sub> (LCO, 1C= 140 mA h g<sup>-1</sup>), LiFePO<sub>4</sub> (LFP, 1C= 170 mA h g<sup>-1</sup>), and LiNi<sub>0.9</sub>Co<sub>0.05</sub>Mn<sub>0.05</sub>O<sub>2</sub> (NCM90, 1C= 200 mA h g<sup>-1</sup>), mixed with carbon black (Super P) and PVDF in a 90:5:5 ratio. The anode was made of commercial graphite (1C= 360 mA h g<sup>-1</sup>), following the same preparation method. Subsequently, an appropriate amount of N-methyl pyrrolidone (NMP) solvent was added to form a uniform slurry. The slurry was then coated onto aluminum and copper collectors for cathode and anode, respectively. After drying and roll pressing, the electrodes were punched into disk shapes with a diameter of 14 mm and subjected to an additional 8 hours of vacuum drying at 120°C. The resulting cathodes featured an

active material mass loading of 4.8 to 5.2 mg cm<sup>-2</sup>, while the anode material had a mass loading of 3.2 to 3.5 mg cm<sup>-2</sup> (according to N/P values of ~1.2).

### **Material Analysis**

All samples underwent structural identification via X-ray diffraction (XRD, Bruker D8, Japan) within a 10° C to 70° C scanning range at a 5° C/min rate. Chemical compositions were scrutinized using X-ray photoelectron spectroscopy (XPS, Al-K $\alpha$ , Thermo Fisher Scientific, USA). The mechanical strength of the MOF-membrane was evaluated by acquiring Young's modulus morphologies using commercial Atomic Force Microscopy (AFM, Bruker Dimension Icon). X-ray absorption fine structure (XAFS) spectroscopy was carried out using the *RapidXAFS* 2M (Anhui Absorption Spectroscopy Analysis Instrument Co., Ltd.) by transmission (or fluorescence) mode at 15 kV and 25 mA. Morphological features were visualized through scanning electron microscopy (SEM, Zeiss Gemini 500, Germany) and high-resolution transmission electron microscopy (HRTEM, JEM-2100, Japan). Barrett-Joyner-Halenda (BJH) and Brunauer-Emmett-Teller (BET) methods (3H-2000PS1/2, Beijing Beishide Instrument-S&T Co., Ltd., China) were utilized to assess the specific surface area and porosity of the samples. To monitor the dynamic changes in polymer functional groups during electrolyte charging and discharging, in-situ Raman spectroscopy (RM-1000, Renishaw) and in-situ Fourier transform infrared spectroscopy (FTIR, Nicolet IS10, USA) were employed. Lithium dendrite growth was directly observed using an optical microscope (Zoom 650, Shanghai Tuming Optical Instrument Co., Ltd.). Lastly, the gassing behavior of the cells was analyzed through an in-situ differential electrochemical mass spectrometry (DEMS) system (HPR-20, Hiden Analytical Ltd.), with argon serving as the inert carrier gas.

### **Electrochemical Measurements**

Ionic conductivity measurement: A coin-cell configuration (CR 2025) was assembled by sandwiching the solid-state electrolyte between two stainless steel electrodes. Electrochemical Impedance Spectroscopy (EIS) tests were conducted using the CHI760E electrochemical workstation from Shanghai Chenhua Instrument Co., Ltd.

These tests spanned a frequency range of 0.1-100 kHz under Open Circuit Potential (OCP) conditions. The ionic conductivity ( $\sigma$ ) was then derived using the following formula:

$$\sigma = l / AR$$

where  $\sigma$  represents the ionic conductivity (measured in S/cm),  $l$  denotes the thickness of the membrane (in cm),  $A$  is the area of the stainless-steel electrode (in cm<sup>2</sup>), and  $R$  signifies the bulk resistance (in  $\Omega$ ).

Li-ion transfer number: The battery configuration consisted of the electrolyte being sandwiched between two lithium metal electrodes (Tianjin China Energy Lithium Co., Ltd. (China)) in coin-cell assemblies. The lithium-ion transference number ( $t_{Li^+}$ ) of solid-state electrolytes was measured using chronoamperometry with a constant potential step of 10 mV. The  $t_{Li^+}$  value was subsequently calculated according to the provided equation:

$$t_{Li^+} = \frac{I_s(\Delta V - I_0 R_0)}{I_0(\Delta V - I_s R_s)}$$

where  $t_{Li^+}$  denotes the lithium-ion transference number.  $I_s$  represents the steady-state current and  $I_0$  the initial current (both in mA).  $R_0$  and  $R_s$  signify the bulk resistances (in  $\Omega$ ), while  $\Delta V$  corresponds to the constant potential applied, which is equal to 10 mV.

Electrochemical window measurement: The battery assembly, featuring an electrolyte sandwiched between a stainless steel electrode and a lithium metal electrode, was used for linear sweep voltammetry (LSV) measurement on an electrochemical workstation. The test conditions were set at a voltage range from 2.5 V to 6 V and a scanning rate of 1 mV/s.

Electrochemical testing of lithium plating/stripping: To examine the effect of solid-state electrolytes on the behavior of lithium metal anodes, constructing symmetric Li//Li and asymmetric Li//Cu cells, both equipped with lithium electrodes having a diameter of 15.0 mm and a thickness of 0.5 mm. For subsequent ex-situ scanning electron

microscopy (SEM) examination, the cells were carefully dismantled inside an argon-filled glovebox and thoroughly cleaned using dimethyl ether (DME).

Electrochemical testing of solid lithium metal button batteries: These coin-cells were assembled using three types of cathodes (LCO, LFP, and NCM90), lithium metal anodes (diameter: 15 mm, thickness: 0.5 mm), and the as-prepared functional solid-state electrolytes. Each coin cell contained 40 microliters of electrolyte. Galvanostatic charge/discharge profiles were conducted on NEWARE battery test system (CT-4008-5V50mA-164 laboratory instrument) at 30°C.

### **Computational Methods**

We performed the first-principles calculations in the frame of density functional theory (DFT) with the program package CASTEP [S1, S2], using the plane-wave ultra-soft pseudopotential (PW-USPP) method and the Perdew-Burke-Ernzerhof (PBE) form of generalized-gradient approximation (GGA) exchange-correlation energy functional [S3]. The structure optimization of MOF has been carried out using means of the Broyden-Fletcher-Goldfarb-Shanno (BFGS) algorithm by relaxing lattice parameters and atomic positions. They would stop until the total energies were converged to  $10^{-5}$  eV/atom, the forces on each unconstrained atom were smaller than  $0.03$  eV/Å, the stresses were lower than  $0.05$  GPa and the displacements were less than  $0.001$  Å. The plane-wave cutoff,  $E_{\text{cut}}$ , was chosen to  $340$  eV. The k-point mesh of  $1 \times 1 \times 1$  was used for Brillouin zone (BZ) sampling.

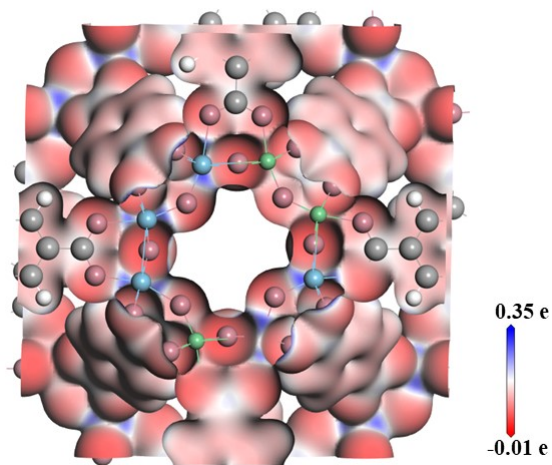


**Fig. S1** ESP of MOFs(Co-Ti) from a top-down perspective.

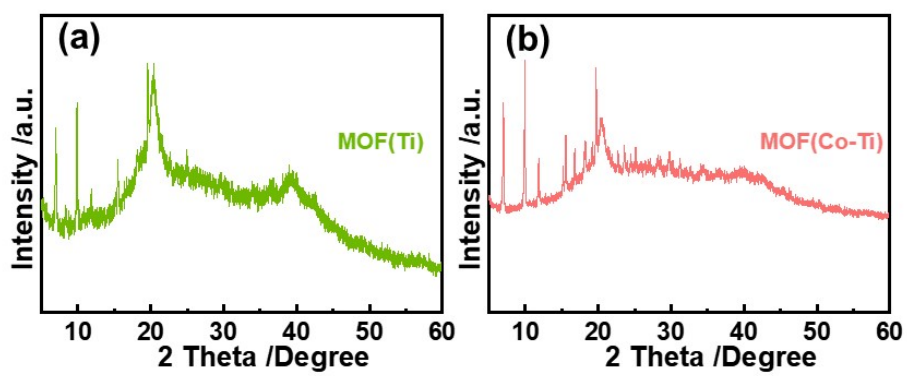


**Fig. S2** The XRD of the as-prepared (a) MOFs(Ti) and (b) MOFs(Co-Ti).

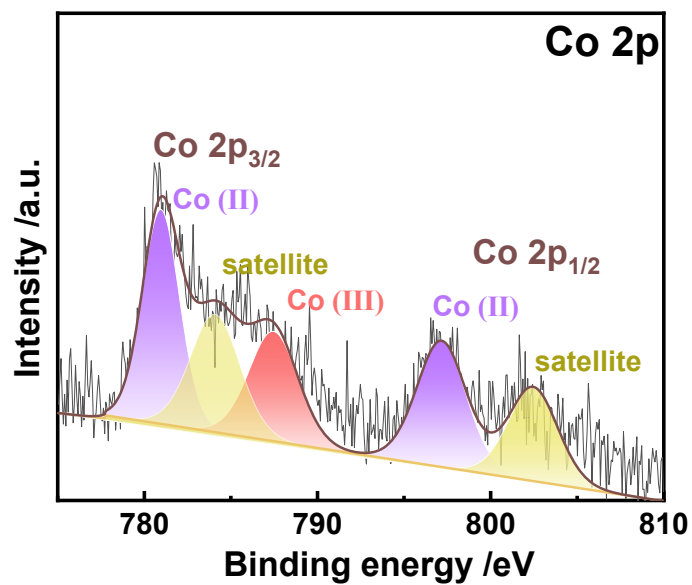


Fig. S3 The XPS spectra of Co 2p for MOFs(Co-Ti).

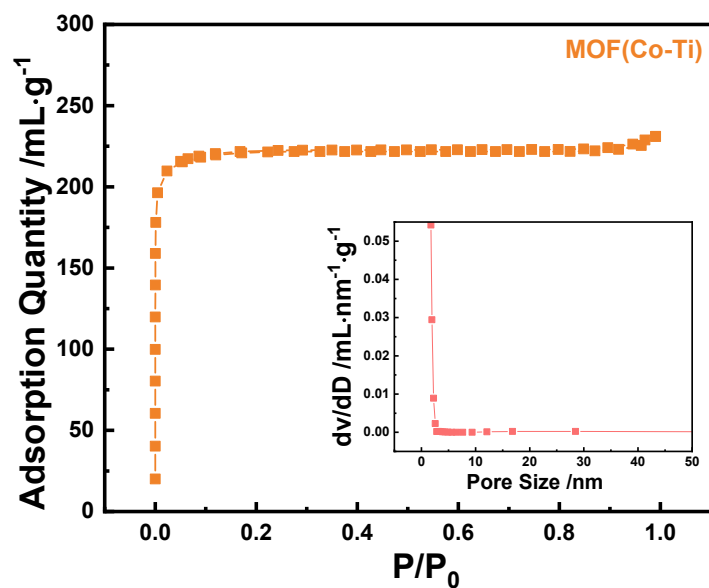
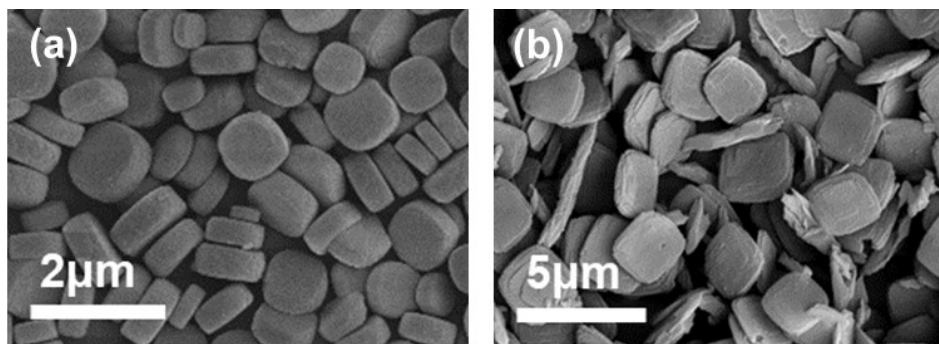
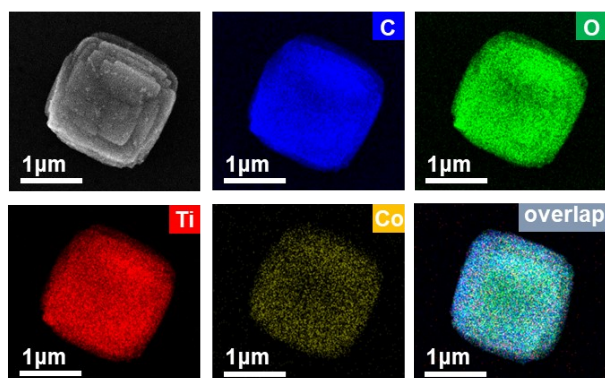


Fig. S4 The BET curves of MOF(Co-Ti) powders.



**Fig. S5** The SEM image of (a) MOFs(Ti) and (b) MOFs(Co-Ti).



**Fig. S6** The TEM-EDS mapping of MOFs(Co-Ti).

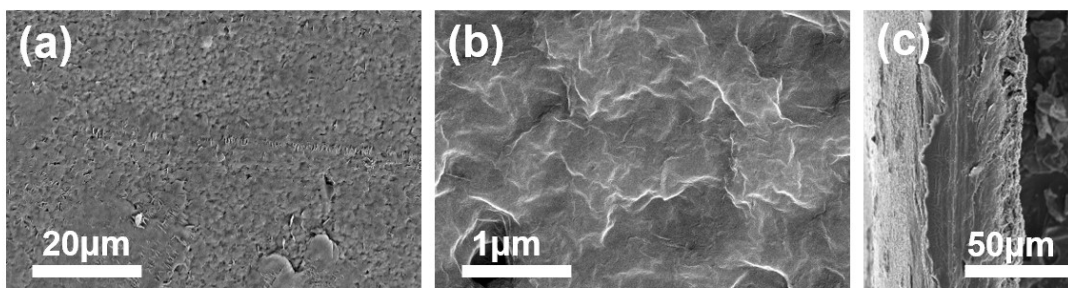


**Fig. S7** SEM morphology of MOF(Ti) membrane.

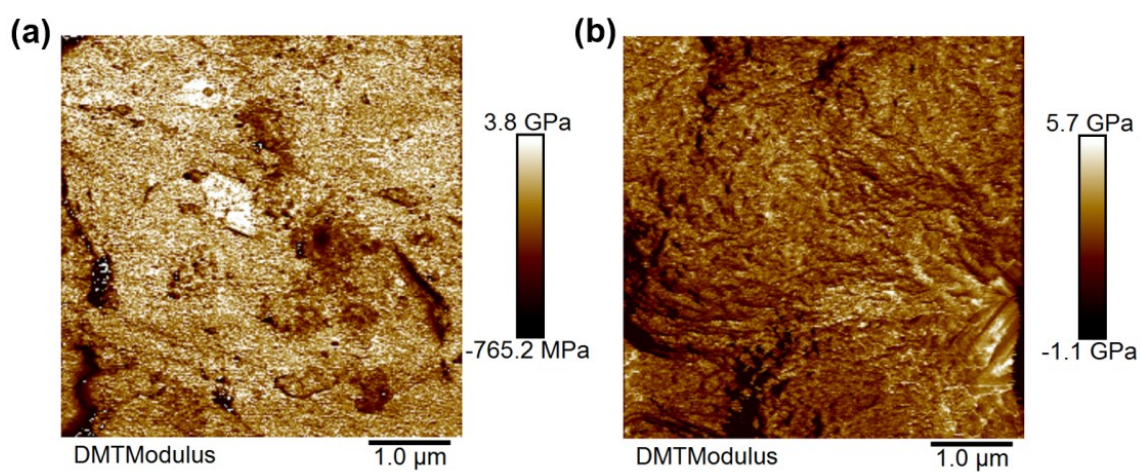


**Fig. S8** Young's modulus image of (a) MOF(Ti) and (b) MOF(Co-Ti).

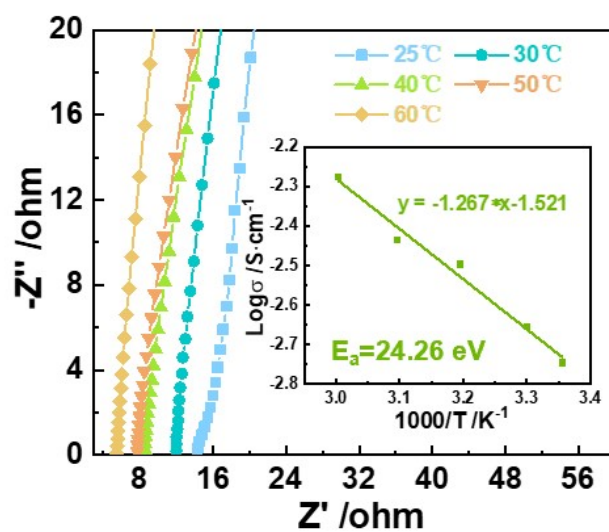


Fig. S9 Ionic conductivities of G@MOF(Ti) at 25-60 °C (the corresponding Arrhenius plot in inset).

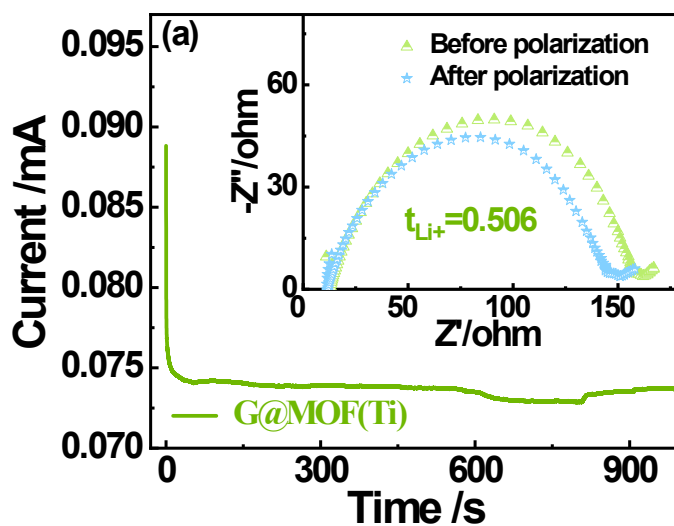


Fig. S10 Chronoamperometric curves of G@MOF(Ti) (inset displays the EIS curves before and after polarization).

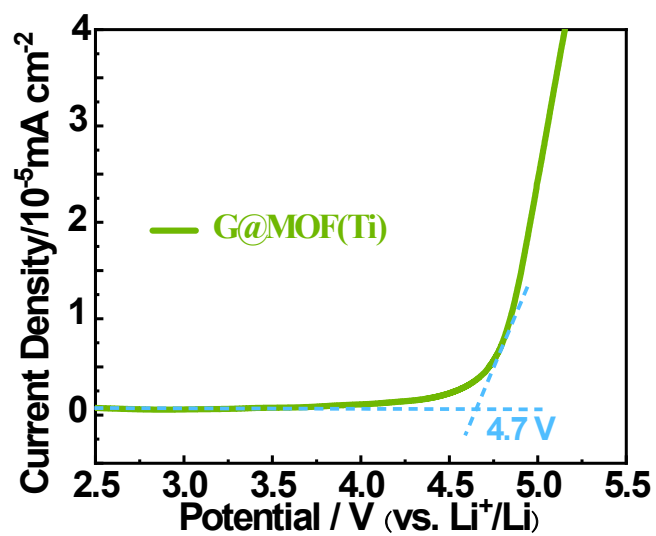


Fig. S11 The LSV curves of G@MOF(Ti).

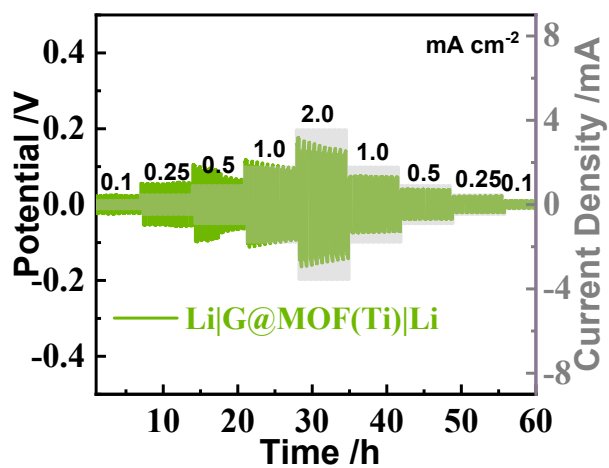


Fig. S12 The Li|Li symmetric cell rate performance of G@MOF(Ti).

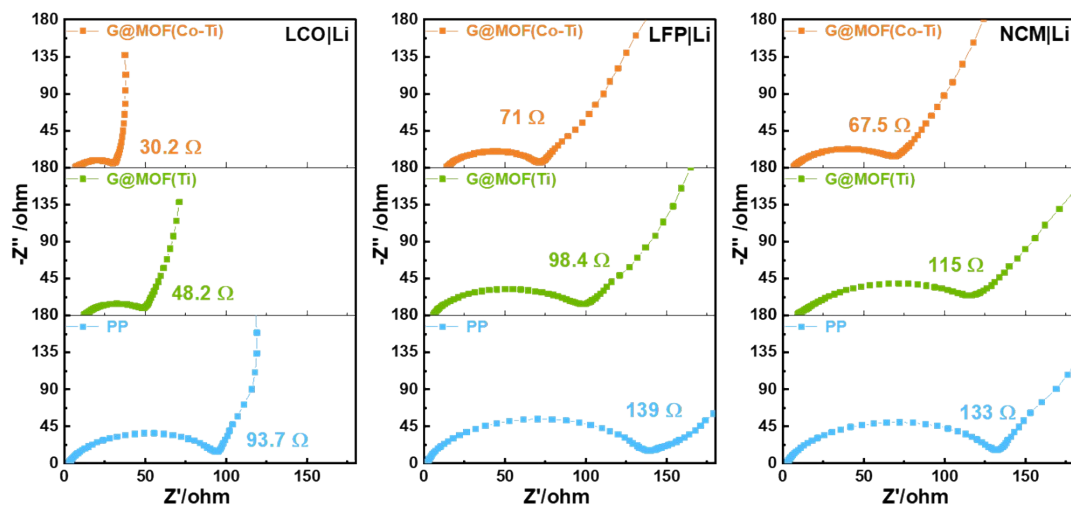


Fig. S13 The EIS of LCO||Li, LFP||Li and NCM90||Li cells.

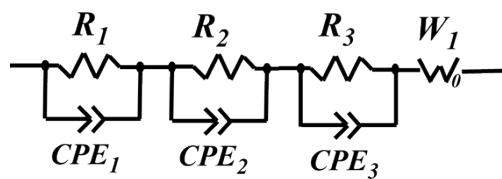


Fig. S14 The equivalent circuits of the LFP||Li cells.

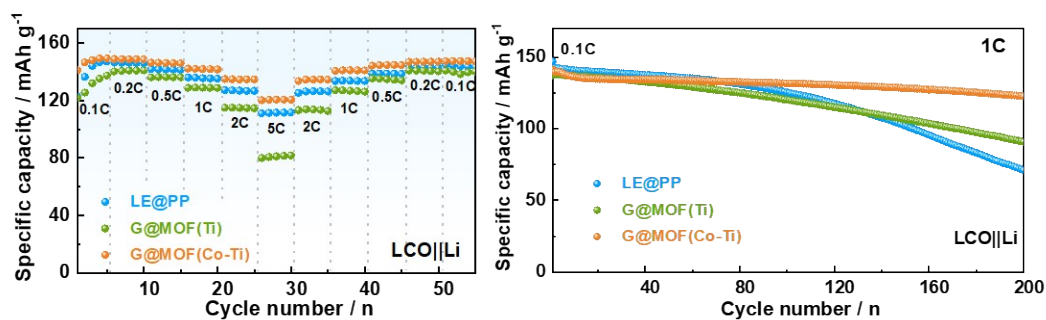
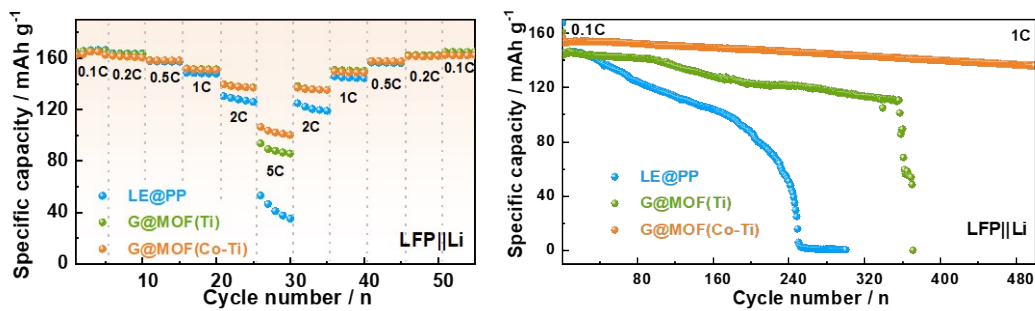
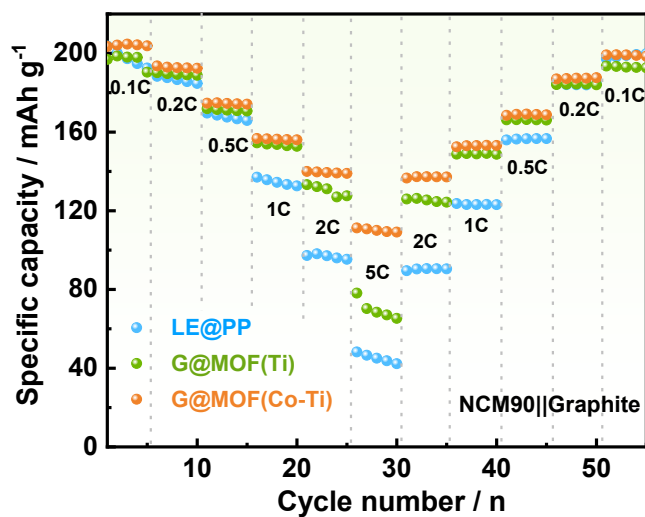


Fig. S15 The rate and long cycle performance of LCO||Li batteries of LE@PP, G@MOF(Ti) and G@MOF(Co-Ti).



**Fig. S16** The rate and long cycle performance of LFP||Li batteries of LE@PP, G@MOF(Ti) and G@MOF(Co-Ti).



**Fig. S17** The rate performance of NCM90||Graphite batteries of LE@PP, G@MOF(Ti) and G@MOF(Co-Ti).

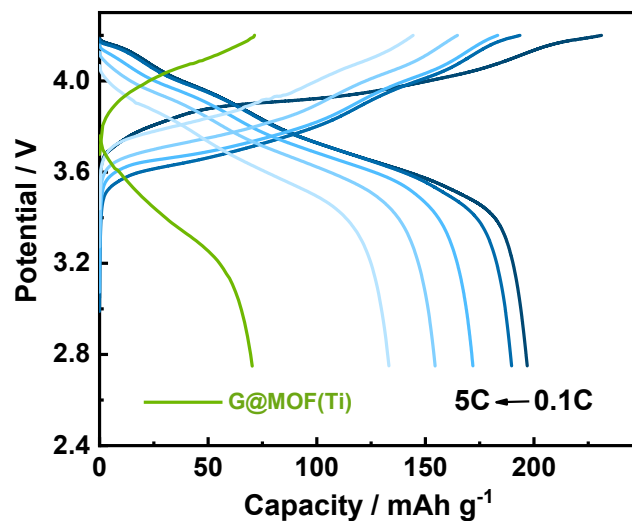


Fig. S18 The voltage platform of G@MOF(Ti).

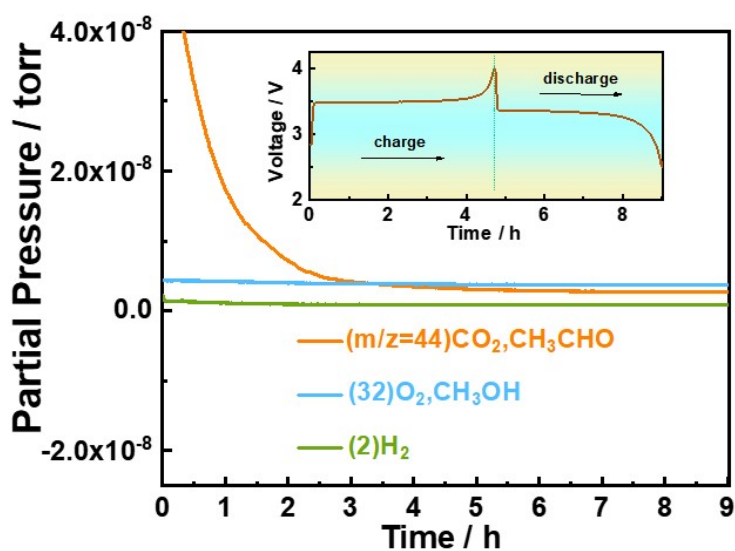
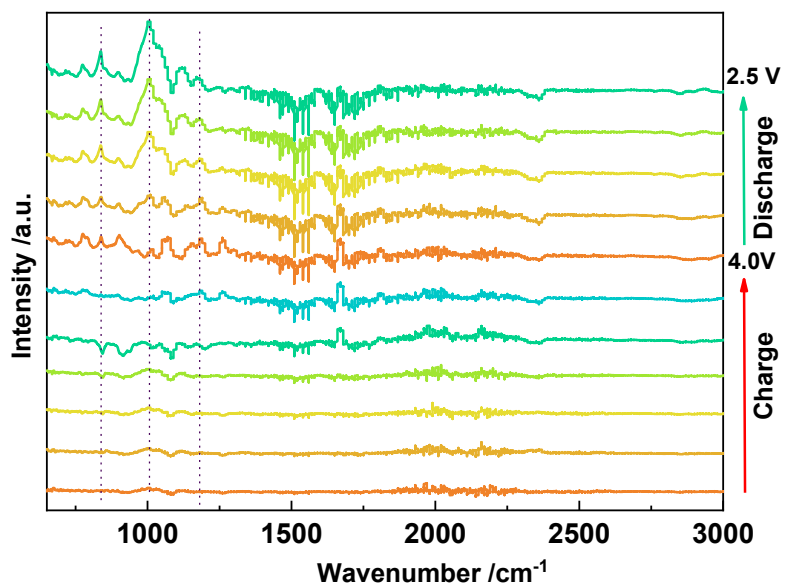
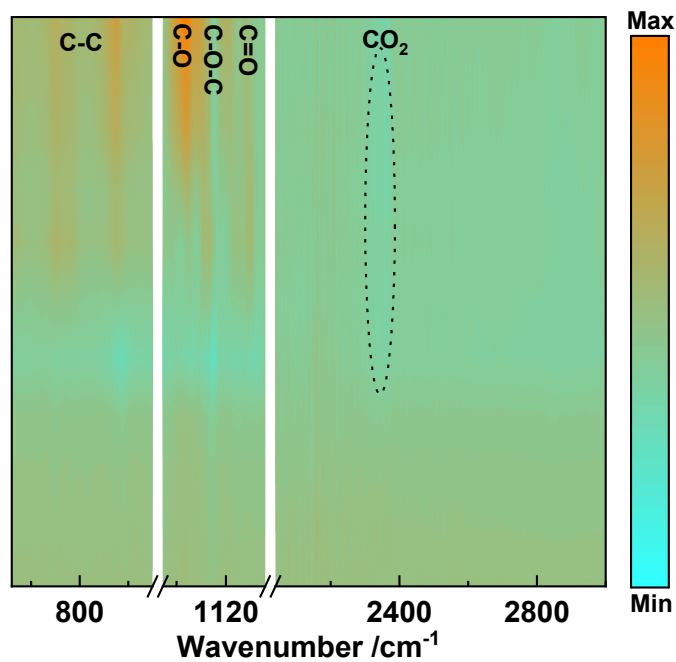


Fig. S19 Various gas generation profiles of the G@MOF(Ti) electrolyte were tested by in situ DEMS.



**Fig. S20** The in-situ FTIR spectroscopy curves of G@MOF(Ti) during the initial discharge-charge cycle.



**Fig. S21** The contour plots of the in situ FTIR spectroscopy for G@MOF(Ti).

**Fig. S22** The galvanostatic charge/discharge and in-situ Raman patterns curves of G@MOF(Ti) during the initial discharge-charge cycle.

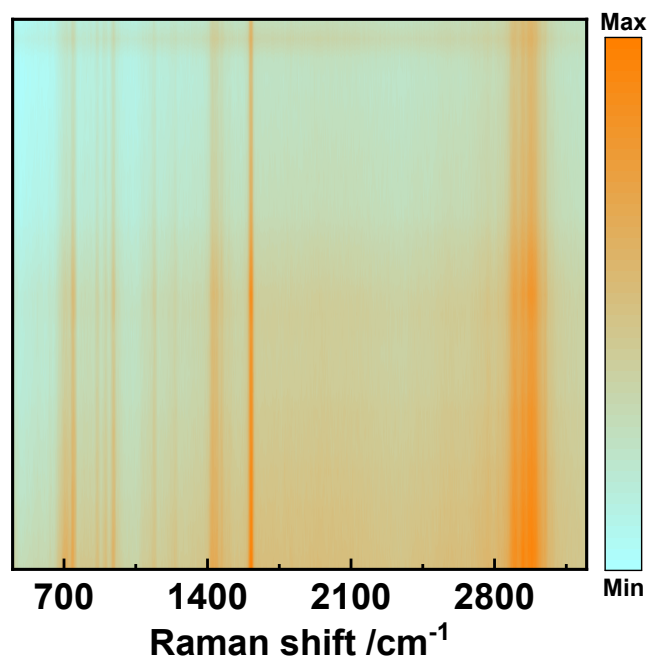


**Fig. S23** The contour plots of the in situ Raman patterns for G@MOF(Ti).

**Table S1** Quantitative fitting results of Co K-edge EXAFS.

sample	Pair	CN	R (Å)	$\sigma^2$ ( $10^{-3}\text{Å}^2$ )	$\Delta E_0$ (eV)	R factor
Co foil	Co-Co	12	2.50	7.0	7.1	0.006
	Co-O	2.2	2.01	2.7	2.0	
MOF(Co)	Co-O	3.6	2.14	3.1	2.0	0.02
	Co-O-Co/Ti	1.1	2.84	9.1	-8.2	

**Table S2** Quantitative fitting results of Ti K-edge EXAFS.

sample	Pair	CN	R (Å)	$\sigma^2$ ( $10^{-3}\text{Å}^2$ )	$\Delta E_0$ (eV)	R factor
Ti foil	Ti-Ti	12	2.92	9.1	5.5	0.01
	Ti-O	2.5	1.84	3.0	10.5	
MOF(Ti)	Ti-O	2.4	2.03	4.4	9.5	0.01
	Ti-O-Ti	1.0	3.04	7.1	-1.9	

**Table S3** Performances comparison with the previously reported electrolyte systems.

Electrolytes	Cathodes	Loading	Rate Performance						Cycle Performance	operating temperature
			(mAh g <sup>-1</sup> )							
		mg cm <sup>-2</sup>	0.1C	0.2C	0.5C	1C	2C	5C	mAh g <sup>-1</sup>	

Uio-66@KANF <sup>[S4]</sup>	LFP	3.0	156.9	156.4	153	148	140	/	150 (1 C, 160 cycles)	30°C
	NCM622		/	/	/	127	/	/	103.4 (1 C, 200 cycles)	
h-PAN@MOF <sup>[30]</sup>	NCM811	4.5	189.7	/	177	166	149	119	140 (0.5 C, 200 cycles)	25°C
MGM-MOFs <sup>[18]</sup>	LFP	3.8	164	160	150	/	/	/	139 (0.2C, 100 cycles)	30°C
	NCM811	3.2	207	200	190	/	/	/	/	
CLA/LATP/LE <sup>[55]</sup>	LFP	/	155	/	/	144	/	/	136(1C, 500 cycles)	25°C
JCSSE/IL <sup>[S6]</sup>	LFP	2.0	152.3	/	/	/	120	/	157 (0.5C, 100 cycles)	25°C
	NCM811	/	/	160	/	/	/	/	140 (0.2C, 100 cycles)	
PTF-4EO <sup>[S7]</sup>	LFP	3.0	162	155	145	131	91	/	131 (0.5C, 200 cycles)	30°C
	NCM721		/	/	/	/	/	/	155 (0.3C, 100 cycles)	
LLZO-CF/PEO <sup>[S8]</sup>	LFP	1.5	149	144.3	142	136	131	123	107 (1C, 500 cycles)	50°C
PAN-PVDF-HFP/Al <sub>2</sub> O <sub>3</sub> /IL <sup>[S9]</sup>	LFP	2.5	157	/	137	123	/	/	133 (0.5C, 500 cycles)	45°C
	NCM811		/	/	120	/	/	/	105 (0.3C, 60 cycles)	
Q-COF <sup>[S10]</sup>	NCM811	/		160					128 (0.2C, 400 cycles)	60°C
This work G@MOF(Co-Ti)	LCO	4.8~5.2	149.3	148	146	141	135	121	122.8 (1C, 200 cycles)	25°C
	LFP		165	161	158	152	138	106	136.8 (1C, 500 cycles)	
	NCM90		225	211	186	163	134	91	138.5 (1C, 200 cycles)	

## References

[S1] M. D. Segall, P. J. D. Lindan, M. J. Probert, C. J. Pickard, P. J. Hasnip, S. J. Clark, M. C. Payne, *J. Phy. Condens. Mat.* **2002**, 14, 2717-2744.

- [S2] S. J. Clark, M. D. Segall, C. J. Pickard, P. J. Hasnip, M. I. J. Probert, K. Refson, M. C. Payne, *Cryst. Mater.* **2005**, 220, 567-570.
- [S3] J. P. Perdew, J. A. Chevary, S. H. Vosko, K. A. Jackson, M. R. Pederson, D. J. Singh, C. Fiolhais, *Phys. Rev. B* **1992**, 46, 6671-6687.
- [S4] Y. X. Liu, Y. X. Liu, S. Q. Wang, W. C. Chen, W. H. Kong, S. P. Wang, H. X. Liu, L. Ding, L.-X. Ding, H. H. Wang, *Adv. Mater.* **2024**, 36, 2401837.
- [30] Y. T. Ma, Y. Qiu, K. Yang, S. Lv, Y. H. Li, F. An, G. Y. Xiao, Z. Han, Y. T. Ma, L. K. Chen, D. F. Zhang, W. Lv, Y. Tian, T. Z. Hou, M. Liu, Z. Zhou, F. Y. Kang, Y. B. He, *Energy Environ. Sci.*, **2024**, 17, 8274-8283.
- [18] Y. F. Xie, L. L. Xu, Y. Tong, Y. Ouyang, Q. H. Zeng, D. X. Li, Y. B. Xiao, S. T. Yu, X. L. Liu, C. Zheng, Q. Zhang, S. M. Huang, *Adv. Mater.* **2024**, 36, 2401284.
- [S5] D. Wang, H. Xie, Q. Liu, K. X. Mu, Z. N. Song, W. J. Xu, L. Tian, C. Z. Zhu, J. Xu, *Angew. Chem. Int. Ed.* **2023**, 62(25), e202302767.
- [S6] Q. Q. Ruan, M. Yao, J. F. Lu, Y. L. Wang, J. Kong, H. T. Zhang, S. J. Zhang, *Energy Storage Mater.* **2023**, 54, 294-303.
- [S7] H. Li, Y. F. Du, Q. Zhang, Y. Zhao, F. Lian, *Adv. Energy Mater.* **2022**, 12, 2103530.
- [S8] P. Pan, M. M. Zhang, Z. L. Cheng, L. Y. Jiang, J. T. Mao, C. K. Ni, Q. Chen, Y. Zeng, Y. Hu, K. (K.) Fu, *Energy Storage Mater.* **2022**, 47, 279-287.
- [S9] D. C. Zhang, Z. B. Liu, Y. W. Wu, S. M. Ji, Z. X. Yuan, J. Liu, M. Zhu, *Adv. Sci.* **2022**, 9, 2104277.
- [S10] C. Q. Niu, W. J. Luo, C. M. Dai, C. B. Yu, Y. X. Xu, *Angew. Chem. Int. Ed.* **2021**, 60, 24915-24923.